CrystEngComm

Accepted Manuscript

ROYAL SOCIETY OF CHEMISTRY

www.rsc.org/crystengcomm

Novel core-shell structured $BiVO_4$ hollow spheres with an ultra-high surface area as visible-light-driven catalyst

Yang Lu,[a] Yong-Song Luo, [a,b,*] Hong-Mei Xiao,[a] Shao-Yun Fu [a, *]

[†]Technical Institute of Physics and Chemistry, Chinese Academy of Sciences, Beijing 100190, China

[‡]Department of Physics and Electronic Engineering, Xinyang Normal University, Xinyang 464000, China

In recent years, $BiVO_4$ has been extensively studied as a promising visible-light-driven catalyst candidate due to its great visible-light absorbing ability. In this paper, novel core-shell structured (CSS) $BiVO_4$ hollow spheres with an ultra-high specific surface area were synthesized via a one-pot, surfactant- and template-free hydrothermal route. The as-obtained products were characterized by scanning electron microscopy, X-ray diffraction, nitrogen adsorption-desorption experimentation, Raman and UV-vis absorption spectroscopy, respectively. The formation mechanism of the $BiVO_4$ products was proposed in terms of the morphological evolution with prolonging the reaction time. The as-prepared CSS $BiVO_4$ hollow spheres similar to Russian dolls were comprised of an inner core and an open outer shell, leading to an ultra-high specific surface area about fifty times as that of solid spherical counterparts fabricated by the traditional solid-state reaction method. As a result, the CSS $BiVO_4$ hollow spheres exhibited a superior photocatalytic activity over not only solid $BiVO_4$ spheres but also other morphological products such as biscuits and plates in the photodegradation of rhodamine B under visible-light irradiation.

* Corresponding author. Tel.: +86 10 82543752; fax: +86 10 82543752.

E-mail address: syfu@mail.ipc.ac.cn (S. Y. Fu), ysluo@xynu.edu.cn.

1. Introduction

Inorganic micro-/nanomaterials with hollow interior spaces are adequate for applications in catalysis, drug delivery, biosensors, gas storage and various advanced applications owing to their high specific surface area, low density, high pore volume and prominent permeability.[1-4] Thus, a variety of chemical and physicochemical methods, such as conventional hard and soft templating, sacrificial templating and template-free synthetic methods etc., have been developed to syntehsize inorganic hollow micro- and nano-structures.[5-10] $BiVO_4$ is one of the most attractive metal vanadates, which has been widely applied in gas sensor, solid-state electrolyte, posistor, positive electrode material and nontoxic yellow pigment, etc..[11-14] Also, it has a great potential for applications in photocatalytic degradation of harmful pollutants.[15-20] So far, $BiVO_4$ products with different morphologies such as one-dimensional nanofibrous and nanotubes,[21,22] two-dimensional nanosheets,[23] three-dimensional flower-like and dendrite-like hierarchical frameworks[24,25] have been got. However, limited work has been done on synthesis of hollow $BiVO_4$ microspheres.[3,26] The hollow olive-shaped $BiVO_4$ microspheres were prepared using the sodium bis(2-ethylhexyl)sulfosuccinate-assisted mixed solvothermal route.[3] The hollow $BiVO_4$ spheres were synthesized using an ultrasonic spray pyrolysis method.[26] Due to their relatively high specific areas, the hollow $BiVO_4$ spheres showed promising photocatalytic activity.[3,26]

In this work, novel core-shell-structured (CSS) $BiVO_4$ hollow spheres with loosed surfaces, which are similar to Russian dolls (namely a set of wooden dolls of decreasing size placed one inside the other), are synthesized using a facile one-pot, surfactant- and template-free hydrothermal process. The total surface of a CSS sphere is comprised of three parts: shell surface, inner-shell surface and core surface. Due to their particular structure, the total surface area of the CSS hollow spheres would be higher than that of other morphological and simple

hollow spherical counterparts. It is well known that the photocatalytic activity of semiconductor photocatalysts is strongly affected by the morphology and the specific surface area.[27-30] The photodegradation of RhB under visible light irradiation is measured to investigate the photocatalytic activity of the as-prepared $BiVO_4$ samples. It will be confirmed if the CSS $BiVO_4$ hollow spheres exhibit superior photocatalytic performance over other morphological products.

2. Experimental section

2.1 Materials and synthesis

All the reagents of analytical grade were purchased from Beijing Chemical Reagent Ltd. and used without further purification. A total of 1 mmol of NH_4VO_3 was added to the 20 ml mixed solvent of CH_3COOH and C_2H_5OH with a volume ratio of 3 : 1, which was marked as solution A. The obtained solution was sonicated in an ultrasonic water bath for 60 min. In the meantime, 1 mmol of $Bi(NO_3)_3 \cdot 5H_2O$ was introduced into the 15 ml mixed solution of C_2H_5OH and CH_3COOH with a volume ratio of 1 : 2 under agitation, and the obtained solution was marked as solution B. After they were completely dissolved, the solution A was added dropwise to the solution B and the obtained mixture was kept stirring for another 30 min until it became homogeneous. Then, the suspension was transferred into a Teflon-lined stainless steel autoclave of 50 ml capacity and heated for 10 h at 180 ^{o}C. After the autoclave was naturally cooled to room temperature, final products were collected and washed several times with ethanol and deionized water, and finally dried in an electric oven for 12 h at 60 ^{o}C. During the course of the reaction, the pH value of the solution was kept at 2 via monitoring by a digital pH-meter. In the synthesis, 246.2 milligrams of the product was obtained and the percent yield was 76% determined in terms of the ratio of the actual yield to the theoretical yield.

2.2 Characterization and measurement

X-ray powder diffraction (XRD) patterns of the products were obtained on a D8 Focus (Bruker, Germany) automated X-ray diffractometer with Cu-Kα radiation (λ=1.5418 Å). Scanning electron microscopy (SEM) images and X-ray energy dispersive spectroscopy (EDS) analysis were carried out on a HITACHI S-4300 electron microscope (Japan) operated at 10 kV acceleration voltage on platinum coated samples. Specific surface area measurements were conducted at 77 K with Quadrasorb SI-MP Surface Area and Porosity Analyzer (American, Quantachrome) via the Brunauer-Emmett-Teller (BET) method with nitrogen adsorption. UV-Vis diffuse reflectance spectroscopy analysis was conducted using Cary 5000 UV-Vis spectrometer equipped with an integrating sphere. The Raman scattering measurement with shifts ranging from 100 to 2000 cm^{-1} was made with a laser Raman spectrometer (Renishaw, England) at room temperature.

The alkaline fluorescent dye rhodamine B (RhB) is widely used for investigating catalytic activity[31-33] and was chosen in this work as a representative type pollutant to evaluate the photocatalytic performance of the $BiVO_4$ products. A 500 W Xe lamp with a cut-off filter (λ > 400 nm) was used as a light source to provide visible light irradiation. Experiments were implemented at ambient temperature as follows: 0.3 g of the photocatalyst was fed into 600 ml of RhB solution (10^{-5} mol • L^{-1}). Before illumination, the solution was magnetically stirred in the dark for 1 h to reach the adsorption-desorption equilibrium between photocatalysts and RhB. One air pump was used to provide enough oxygen. At given time intervals, 10 ml suspension of RhB solution was monitored by checking the absorbance of solutions at 553 nm during the photodegradation process using a U-3900 spectrophotometer.

3. Results and discussion

3.1 Crystal structure and composition

Fig. 1 shows the XRD patterns of the samples prepared in a series of time intervals. In Fig. 1a, the starting precursor obtained by inorganic precipitate reaction was amorphous compound before hydrothermal process. As shown in Fig. 1b, the crystalline phase appeared after 1 h hydrothermal treatment. As the hydrothermal process extended from 1 to 15 h, the intensity of diffraction peaks increased gradually. Meanwhile, no peaks of other phases or impurities were detected. All peaks of the XRD patterns shown in Fig.1b-f could be assigned to the monoclinic phase of $BiVO_4$. Lattice parameters derived from this study were in good agreement with the literature data (space group of $BiVO_4$: I2/a; a=5.195 Å, b=11.701 Å, c=5.092 Å, β =90.38^o, mineral name: clinobisvanite, JCPDS file NO. 14-0668). The refined lattice constants obtained from the XRD result are given in Table 1. The EDS analysis shown in Fig. 2 reveals that the elemental composition of the obtained $BiVO_4$ products consist of only bismuth, vanadium, and oxygen, indicating the high purity of the products. The ratio of Bi : V atoms is approximately 1 : 1.06 and the ratio of Bi: V: O is approximately equal to 1 : 1 : 4, which are consistent with the stoichiometric ratios of $BiVO_4$.

3.2 Morphology and microstructure

The morphology and microstructure of the $BiVO_4$ samples were investigated by scanning electron microscopy. Fig. 3 shows typical SEM images of the as-prepared $BiVO_4$ products obtained at 180 ^{o}C after 10 h. The low-magnification SEM image (Fig. 3a) gives the panoramic view and shows that the majority of the crystals possess a uniform Russian-doll-like CSS hollow spherical shape with an average outer diameter of about 8 μm. The close-up view of a CSS

hollow sphere revealed by high-magnification SEM image (Fig. 3b) further demonstrates that the core and the shell are separated and there is a large void space between them. Moreover, the coarse shell (namely loosed surface) of the CSS $BiVO_4$ hollow spheres is actually made of fine particles with the size of about 200 nm and the shell thickness is about 500 nm.

To investigate the formation process and the growth mechanism of $BiVO_4$ products with novel Russian-toll-like core-shell hollow structure, we have carried out time-dependent experiments and inspected the growth process systematically by analyzing the samples collected at different growth periods. Fig. 4a displays that the samples obtained without hydrothermal treatment contain a large amount of irregular nanoparticles and own amorphous property as confirmed by the corresponding XRD pattern (Fig. 1a). When the reaction time was prolonged to 3 h, plentiful solid $BiVO_4$ microspheres were formed, accompanied by some nanoparticles (Fig. 4b). The rough surfaces of these solid $BiVO_4$ microspheres indicate that these particles are formed from nanoparticles. Fig. 4c shows that lots of well-defined sphere-like architectures were produced after hydrothermal reaction for 5 h. And the evacuation of solid spheres commenced at a particular area underneath the immediate skin, separating the original solid sphere into two discrete parts of core and shell. After further extending the reaction time to 10 h, the evacuation continued and the core shrank to form a hollow core-shell structure as shown in Fig. 4d. The resultant void space between the core and the shell was affirmed by Fig. 4d. It is well known that the surfactants are helpful for preventing nanoparticles from aggregation and growth.[34] In the absence of surfactants, big particles with broad size distributions are generally obtained.[35] In this work, no surfactants were employed in synthesizing $BiVO_4$ products. Consequently, the as-synthesized $BiVO_4$ products have a relatively big micro-scale size as shown in Fig. 4.

Nonetheless, it would be interesting in future work to check if any surfactants may be employed for the purpose of controlling and tuning the particle size down to 100 nm.

The close-up views (Fig. 5) of the as-synthesized CSS $BiVO_4$ hollow spheres were conducted to observe the specific growth dynamics. It can be clearly observed that the shell of $BiVO_4$ hollow spheres become thinner with the extension of hydrothermal reaction time. This means that the shell thickness of CSS $BiVO_4$ hollow spheres can be controlled through adjusting the reaction time as shown in Fig. 5a-f. A concise schematic illustration for the process of the shape evolution is shown in Fig. 6. Ostwald ripening is a feasible mechanism for the formation of the CSS $BiVO_4$ hollow spheres.[1] At the initial stage of reaction, the tiny $BiVO_4$ crystallites first aggregate into solid spheres. As the inner crystallites are dissolved, a void that is surrounded by the re-crystallized shell is created. As a result, the void space divides the solid sphere into two separate regions to shape a core-shell structure.

The CSS $BiVO_4$ hollow spheres are expected to have an ultra-large specific surface area due to their particular structure. Nitrogen adsorption-desorption measurement is an appropriate technique for probing the BET surface area and internal pore size distribution. The adsorption and desorption isotherm of the CSS $BiVO_4$ hollow spheres depicts a pregnant hysteresis loop in the relative pressure range of 0.4-1.0 (Fig. 7), which reveals that the $BiVO_4$ sample is a mesoporous material.[36] The BET surface area for the as-prepared products calculated from the linear part of the BET plot is about 13.09 $m^2 g^{-1}$, which is about 50 times as that of the $BiVO_4$ solid spheres by the solid-state reaction (SSR) method[37] and is also much higher than that of the previously reported $BiVO_4$ samples with various morphologies,[3,37-40] and the corresponding result is summarized in Table 2. The corresponding pore size distribution curve calculated from the desorption branch by the Barett-Joyner-Halenda (BJH) method displays a pore size

distribution from 3 to 5 nm, centered at ca.4 nm as shown in the inset of Fig. 7. For the purpose of comparison in photocatalytic activity, other morphological $BiVO_4$ samples were also synthesized. All of the experiment conditions remain unchanged, 0.5 g CTAB or 0.5 g PVP was added to the solution B before solution mixing, finally plate-like and biscuit-like $BiVO_4$ samples were obtained, respectively (Fig. 8).

Raman spectroscopy has been certified very useful for exploring local structure of materials, since the coordination environment of specific atoms in the structure can be verified immediately from the Raman vibrational spectrum.[41-43] Fig. 9 shows the Raman spectrum of the 150-1000 cm^{-1} region of the CSS $BiVO_4$ sample. The peaks around 209, 327, 367, 713, and 824 cm^{-1} were observed, which are the typical vibrational bands of $BiVO_4$.[44,45] The 209 cm^{-1} band is the external mode (rotation/translation). The asymmetric and symmetric transformation modes of the VO_4^{3-} tetrahedron are near 327 and 367 cm^{-1}, respectively. The most intense peak at 824 cm^{-1} and the weak shoulder at about 713 cm^{-1} are attributed to the stretching modes of two adverse types of V-O bonds.

3.3 UV-Vis diffuse reflectance spectrum and band gap

Diffuse reflectance spectroscopy is an appropriate implement to depict the energy band structure feature of a semiconductor, which is relevant to the optical absorption property considered as a pivotal factor in determining its photocatalytic activity.[46] Fig. 10 shows the UV-Vis diffuse reflectance spectra of $BiVO_4$ samples. The $BiVO_4$ microspheres present intense absorption in the visible region until ~525 nm in addition to that in the UV light region. The steep shape of spectra revealed that the visible light absorption is not due to the transition from impurity levels but to the band gap transition.[47] For the monoclinic scheelite $BiVO_4$, the visible absorption band is designated to the transition from a valence band formed by Bi_{6s} or a hybrid orbital of Bi_{6s} and

O_{2p} to a conduction band of V_{3d}.[18] The band gap (E_g) of the sample can be estimated according to formula $ahν = A(hν - E_g)^{n/2}$,[48] where a, h, ν, A and E_g are the absorption coefficient, Planck's constant, the incident light frequency, a constant and the band-gap energy, respectively. For $BiVO_4$, the value of n is 1, which indicates that $BiVO_4$ is a direct band gap material.[39,49] The plots of $(ahν)^2$ versus photonenergy (hν) are shown in the inset of Fig. 10, from which we could estimate the energy of the band gap of $BiVO_4$ sample. The estimated E_g of plate-like $BiVO_4$, biscuit-like $BiVO_4$, and CSS $BiVO_4$ hollow spheres from the intercept of the tangents to the plots were 2.46, 2.48 and 2.43 eV, respectively, which demonstrates that the as-obtained samples have adequate band gaps for photocatalytic decomposition of organic pollutants under visible-light irradiation.

3.4 Photocatalytic activity

In order to survey the photocatalytic activity of the as-obtained $BiVO_4$ products, RhB with a major absorption band at 553 nm, was selected as the model pollutant. Temporal evolution of the spectral change during the photodegradation of RhB over the CSS $BiVO_4$ hollow spheres under visible-light illumination is exhibited in Fig. 11a. A gradual decrease of RhB absorption accompanied with an absorption band shift to shorter wavelengths is observed with increasing exposure time under irradiation of visible light. After 4.5 h, the major absorption band is shifted from 553 to 498 nm, that is to say, dye's de-ethylation is a stepwise course under visible illumination.

Fig. 11b shows the results of the RhB photodegradation using different catalysts under visible light illumination ($\lambda > 400$ nm). C is the absorption of RhB at the wavelength of 553 nm and C_0 is the absorption after the adsorption-desorption equilibrium between photocatalyst and RhB before irradiation. The blank test (curve A) demonstrates that the photolysis of RhB is

extremely low when there is no photocatalyst, namely merely about 10% of the photodegradation after 4.5 h under visible irradiation. The adsorption of RhB by the CSS $BiVO_4$ hollow spheres in the dark is also inspected. After 4.5 h, the concentration of RhB is decreased by about 30% (curve B), proving that the decolorization of RhB by the as-prepared $BiVO_4$ sample is basically attributed to photodegradation but not adsorption. Curves C~F show that the three morphological $BiVO_4$ samples show different photodegradation efficiencies under visible-light irradiation after 4.5 h. As shown in curve C, the precursor of $BiVO_4$ products is used to degrade RhB solution, the photodegradation efficiency is just 47% after 4.5 h. However, when the as-synthesized $BiVO_4$ samples are dispersed in RhB solution, the photocatalytic activity is obviously enhanced as depicted in curves D~F of Fig. 11b. In comparison, 68%, 88% and 99% of the RhB are degraded after 4.5 h, respectively for the three $BiVO_4$ products of biscuits, plates and CSS hollow spheres. The larger surface area the photocatalysts possess, the higher photocatalytic activity they show. Since the three products of different morphologies are the same material, the outstanding photocatalytic activity can be mainly ascribed to the ultra-high surface area of the CSS $BiVO_4$ hollow spheres, which can supply more surfaces for the photogenerated electrons and holes to contact with the RhB. In addition, the stability of the photocatalytic activity of the CSS $BiVO_4$ hollow spheres is evaluated by five recycling runs in the photocatalytic degradation of RhB under visible-light irradiation. They are repeatedly used in the photocatalytic process with an advantage of easy separation under an external centrifugation. It can be observed that the decrease of the photocatalytic activity is less than 5% after five recycling runs (Fig. 12). The excellent photocatalytic activity and stability of the CSS $BiVO_4$ hollow spheres display that they have a high potential as a promising visible-light driven catalyst candidate for industrial applications.

4. Conclusions

In this work, a simple one-step, surfactant- and template-free hydrothermal route has been developed for the synthesis of the novel core-shell structured (CSS) $BiVO_4$ hollow spheres. From the shape evolution of the time-dependent samples, it is believed that Ostwald ripening is the primary driving force for the core separation from the shell during the hydrothermal process. Photodegradation test of RhB indicates that the as-prepared CSS $BiVO_4$ product exhibits superior photocatalytic activity due to its ultra-high surface area over other morphological counterparts. The facile route presented here uses only common and inexpensive reagents, which makes it suitable for the large-scale production of the CSS $BiVO_4$ with excellent photocatalytic activity and stability as a highly active visible-light driven photocatalyst candidate for industrial applications.

Acknowledgements

The authors acknowledge the financial supports from the National Basic Research Program of China (No. 2010CB934500) and National Natural Science Foundation of China (Nos. 51373187 and 11372312.

Notes and references

1. Z. J. Yang, J. J. Wei, H. X. Yang, L. Liu, H. Liang and Y. Z. Yang, *Eur. J. Inorg. Chem.*, 2010, 3354.

2. Y. Du, Z. X. Cheng, S. X. Dou, D. J. Attard and X. L. Wang, *J. Appl. Phys.*, 2011, **109**, 073903.

3. M. L. Guan, D. K. Ma, S. W. Hu, Y. J. Chen and S. M. Huang, *Inorg. Chem.*, 2011, **50**, 800.

4. S. Z. Qiao, C. X. Lin, Y. G. Jin, Z. Li, Z. M. Yan, Z. P. Han, Y. N. Huang and G. Q. Lu, *J. Phys. Chem. C*, 2009, **113**, 8673.

5. X. W. Lou, Lynden A. Archer and Z. C. Yang, *Adv. Mater.*, 2008, **20**, 3987.

6. Z. Ma and S. Dai, *ACS Catal.*, 2011, **1**, 805.

7. J. Zhou, W. Wu, D. Caruntu, M. H. Yu, A. Martin, J. F. Chen, C. J. O'Connor and W. L. Zhou, *J. Phy. Chem. C*, 2007, **111**, 17473.

8. Nicholas C. Strandwitz and Galen D. Stucky, *Chem. Mater.*, 2009, **21**, 4577.

9. S. J. Liu, Y. F. Hou, S. L. Zheng, Y. Zhang and Y. Wang, *CrystEngComm*, 2013, **15**, 4124.

10. N. Pinna, G. Neri, M. Antonietti and M. Niederberger, *Angew. Chem.*, 2004, **116**, 4445.

11. S. R. Wang, J. Zhang, J. Q. Jiang, R. Liu, B. L. Zhu, M. J. Xu, Y. Wang, J. L. Cao, M. Y. Li, Z. Y. Yuan, S. M. Zhang, W. P. Huang and S. H. Wu, *Microporous Mesoporous Mater.*, 2009, **123**, 349.

12. Y. Zhao, Y. Xie, X. Zhu, S. Yan and S. X. Wang, *Chem. Eur. J.*, 2008, **14**, 1601.

13. K. Shantha and K. B. R. Varma, *Mater. Sci. Eng. B*, 1999, **60**, 66.

14. P. Shuk, H. D. Wiemhofer, U. Guth, W. Gopel and M. Greenblatt, *Solid State Ion.*, 1996, **89**, 179.

15. M. D. Han, X. F. Chen, T. Sun, O. K. Tan and M. S. Tse, *CrystEngComm*, 2011, **13**, 6674.

16. S. Kohtani, M. Koshiko, A. Kudo, K. Tokumura, Y. Ishigaki, A. Toriba, K. Hayakawa and R. Nakagaki, *Appl. Catal. B: Environ.*, 2003, **46**, 573.

17. S. Tokunaga, H. Kato and A. Kudo, *Chem. Mater.*, 2001, **13**, 4624.

18. J. Yu and A. Kudo, *Chem. Lett.*, 2005, **34**, 850.

19. L. Zhou, W. Z. Wang, S. W. Liu, L. S. Zhang, H. L. Xu and W. Zhu, *J. Mol. Catal. A: Chem.*, 2006, **252**, 120.

20. M. Ge, L. Liu, W. Chen and Z. Zhou, *CrystEngComm*, 2012, **14**, 1038.

21. X. F. Zhang, L. L. Du, H. Wang, X. L. Dong, X. X. Zhang, C. Ma and H. C. Ma, *Microporous Mesoporous Mater.*, 2013, **173**, 175.

22. L. Ren, L. Jin, J. B. Wang, F. Yang, M. Q. Qiu and Y. Yu, *Nanotechnology*, 2009, **20**, 115603.

23. L. Zhang, D. R. Chen and X. L. Jiao, *J. Phys. Chem. B*, 2006, **110**, 2668.

24. A. P. Zhang, J. Z. Zhang, *Spectrochimica Acta Part A*, 2009, **73**, 336.

25. L. Zhou, W. Z. Wang and H. L. Xu, *Cryst. Growth. Des.*, 2008, **8**, 728.

26. S. S. Dunkle, R. J. Helmich and K. S. Suslick, *J. Phys. Chem. C*, 2009, **113**, 11980.

27. L. Zhou, W. Z. Wang, H. L. Xu and S. M. Sun, *Cryst. Growth. Des.*, 2008, **8**, 3595.

28. G. H. Tian, Y. J. Chen, W. Zhou, K. Pan, Y. Z. Dong, C. G. Tian and H. G. Fu, *J. Mater. Chem.*, 2011, 21, 887.

29. Y. Lu, Y. S. Luo, D. Z. Kong, D. Y. Zhang, Y. L. Jia, and X. W. Zhang, *J. Solid State Chem.*, 2012, **186**, 255.

30. Y. Jiao, F. F. Wang, X. M. Ma, Q. H. Tang, K. Wang, Y. M. Guo and L. Yang, *Microporous Mesoporous Mater.*, 2013, **176**, 1.

31. M. Shang, W. Z. Wang, S. M. Sun, L. Zhou and L. Zhang, *J. Phys. Chem. C*, 2008, **112**, 10407.

32. Z. X. Chen, D. Z. Li, W. J. Zhang, Y. Shao, T. W. Chen, M. Sun and X. Z. Fu, *J. Phys. Chem. C*, 2009, **113**, 4433.

33. X. J. Dai, Y. S. Lou, W. D. Zhang and S. Y. Fu, *Dalton. Trans.*, 2010, **39**, 1.

34. M. Shang, W. Z. Wang, L. Zhou, S. M. Sun and W. Z. Yin, *J. Hazar. Mater.*, 2009, **172**, 338.

35. X. J. Shen, J. P. Yang, Y. Liu, Y. S. Luo and S. Y. Fu, *New J. Chem.*, 2011, **35**, 1403-1409.

36. J. C. Groen, L. A. A. Peffer and J. Perez-Ramirez, *Microporous Mesoporous Mater.*, 2003, **60**, 1.

37. W. Z. Yin, W. Z. Wang, L. Zhou, S. M. Sun and L. Zhang, *J. Hazar. Mater.*, 2010, **173**, 194.

38. D. N. Ke, T. Y. Peng, L. Ma, P. Can and K. Dai, *Inorg. Chem*., 2009, **48**, 4685.

39. S. M. Sun, W. Z. Wang, Z. Lin and H. L. Xu, *Ind. Eng. Chem. Res.*, 2009, **48**, 1735.

40. Z. Q. Wang, W. J. Luo, S.C. Yan, J. Y. Feng, Z. Y. Zhao, Y. S. Zhu, Z. S. Li and Z. G. Zou, *CrystEngComm*, 2011, **13**, 2500.

41. Ray L. Frost, Dermot A. Henry, Matt L. Weier and Wayde Martens, *J. Raman Spectrosc.*, 2006, **37**, 722.

42. J. Q. Yu and A. Kudo, *Adv. Funct. Mater.*, 2006, **16**, 2163.

43. J. B. Liu, H. Wang, S. Wang and H. Yan, *Mater. Sci. Eng.:B*, 2003, **104**, 36.

44. C. G. Li, G. S. Pang, S. M. Sun and S. H. Feng, *J. Nanopart. Res.*, 2010, **12**, 3069-3075.

45. A. Galembeck and O. L. Alves, *Thin Solid Film*, 2000, **365**, 90.

46. J. W. Tang, Z. G. Zou and J. H. Ye, *Angew. Chem. Int. Ed.*, 2004, **43**, 4463.

47. A. Kudo, I. Tsuji and H. Kato, *Chem. Commun.*, 2002, **48**, 1958.

48. L. Chen, S. F. Yin, R. Huang, Q. Zhang, S. L. Luo and C. T. Au, *CrystEngComm*, 2012, **14**, 4217.

49. L. Zhou, W. Z. Wang, H. L. Xu, S. M. Sun and M. Shang, *Chem. Eur. J.*, 2009, **15**, 1776.

Table 1 The refined lattice constants obtained from the XRD result for the $BiVO_4$ product

Samples	Refined lattice constants (Å)		
	a	b	c
1 h	5.161	11.664	5.102
3 h	5.175	11.672	5.099
5 h	5.175	11.681	5.096
10 h	5.177	11.678	5.099
15 h	5.179	11.693	5.099

Table 2 Specific surface areas of $BiVO_4$ products with different morphologies (SSR: spheres by solid-state reaction method; SS: solid spheres; S-L: star-like; O-L: olive-like; C-L: cubic-like; B-L: biscuit-like; P-L: plate-like; CSS: core-shell double-structured spheres)*

$BiVO_4$ Sample	SSR[37]	SS[38]	S-L[39]	O-L[3]	C-L[40]	B-L	P-L	CSS
Specific surface area($m^2\ g^{-1}$)	0.26	1.04	1.07	1.445	2.3	3.993	4.848	13.09

*Note : B-L, P-L products and CSS hollow spheres were synthesized in 10 h reaction time.

Figure captions

Fig. 1 The XRD patterns of the $BiVO_4$ products: (a) the precursor, (b) 1 h, (c) 3 h, (d) 5 h, (e) 10 h and (f) 15 h.

Fig. 2 EDS profile of the as-prepared $BiVO_4$ products prepared in 10 h reaction time.

Fig. 3 (a) Low-magnification SEM image of the CSS $BiVO_4$ hollow spheres and (b) SEM image of an individual CSS $BiVO_4$ hollow sphere.

Fig. 4 SEM images of the CSS $BiVO_4$ hollow spheres obtained at various reaction times: (a) 0 h, (b) 3 h, (c) 5 h and (d) 10 h.

Fig. 5 The close-up sequence of the evolution of the CSS $BiVO_4$ hollow spheres: (a) 1 h, (b) 3 h, (c) 5 h, (d) 8 h, (e)10 h and (f) 15 h.

Fig. 6 Schematic illustration of the proposed formation mechanism of the CSS $BiVO_4$ hollow spheres.

Fig. 7 N_2 adsorption-desorption isotherm of the CSS $BiVO_4$ hollow spheres. The inset is the corresponding BJH pore size distribution.

Fig. 8 SEM images of $BiVO_4$ products prepared in 10 h reaction time: (a,b) biscuit-like $BiVO_4$ by adding 0.5 g PVP to the solution B before solution mixing; (c,d) plate-like $BiVO_4$ by adding 0.5 g CTAB to the solution B before solution mixing.

Fig. 9 Raman spectrum of the CSS $BiVO_4$ hollow spheres.

Fig. 10 The UV/Vis diffuses reflectance spectra of the $BiVO_4$ samples: (a) $BiVO_4$ biscuits, (b) $BiVO_4$ plates and (c) CSS $BiVO_4$ hollow spheres. The inset is the plots of $(\alpha E_p)^2$ *vs* photon energy (E_p).

Fig. 11 (a) The temporal evolution of the absorption spectra of the RhB solution in the presence of CSS $BiVO_4$ hollow spheres under exposure to visible light and (b) the effect of catalysts on photocatalytic degradation of RhB (initial concentration $=1.0\times10^{-5}$ M).

Fig. 12 Photocatalytic degradation of RhB (initial concentration $=1.0\times10^{-5}$ M) after five recycling runs in the presence of the CCS $BiVO_4$ (0.3 g) under visible-light irradiation.

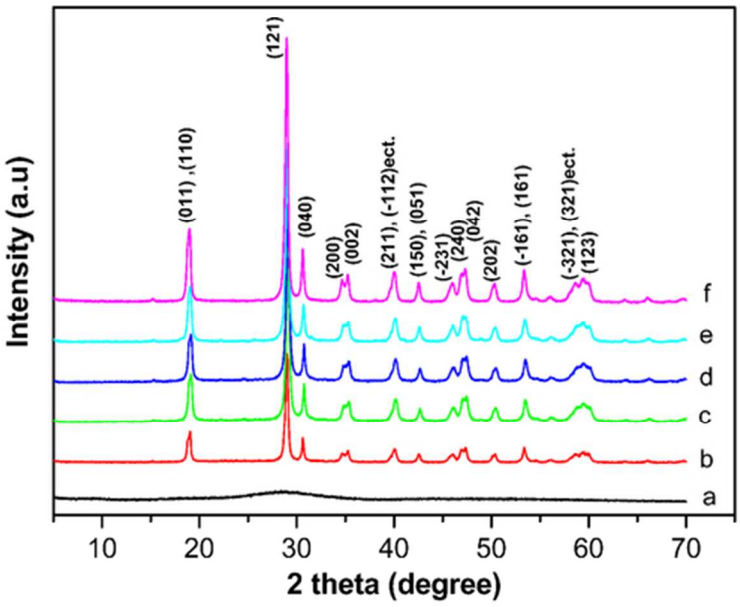

56x39mm (300 x 300 DPI)

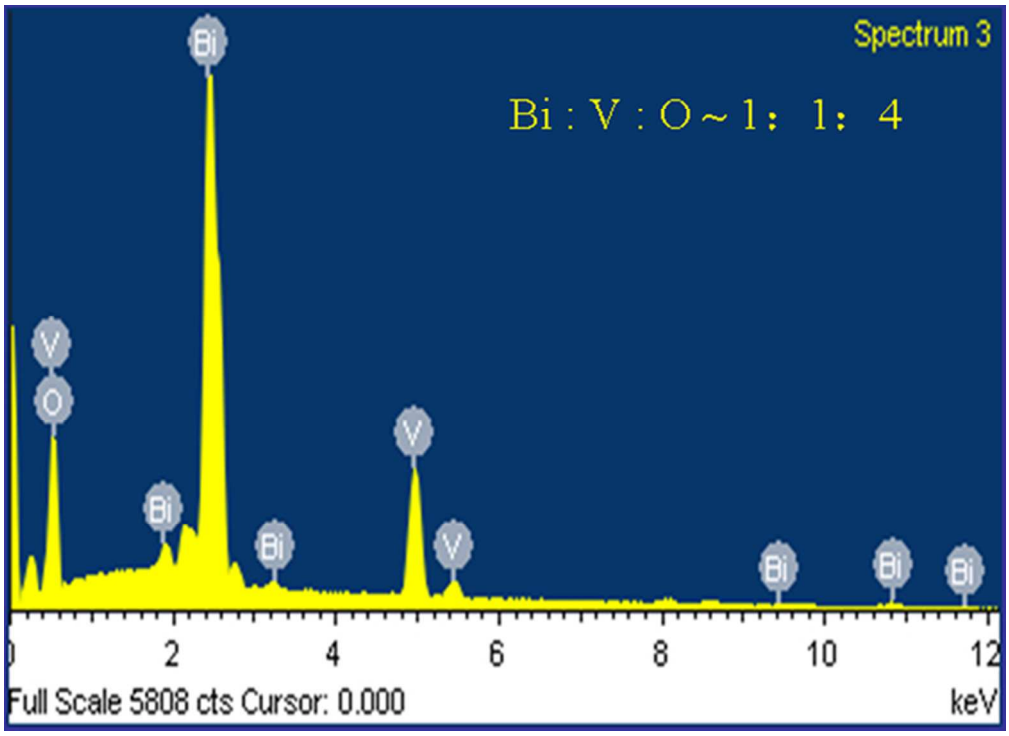

57x42mm (300 x 300 DPI)

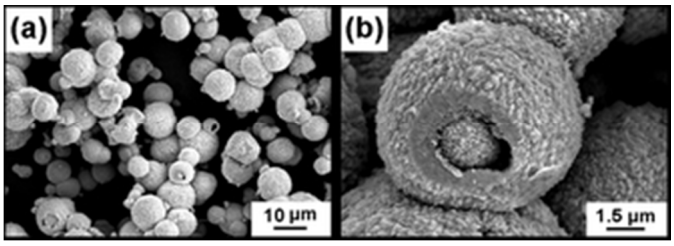

28x9mm (300 x 300 DPI)

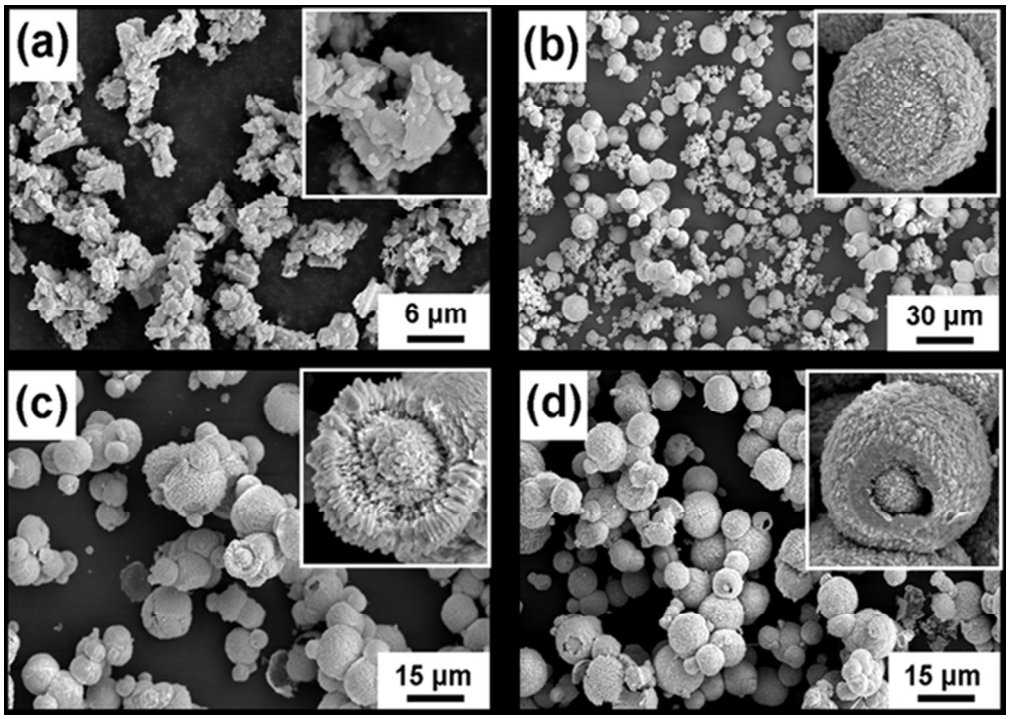

56x40mm (300 x 300 DPI)

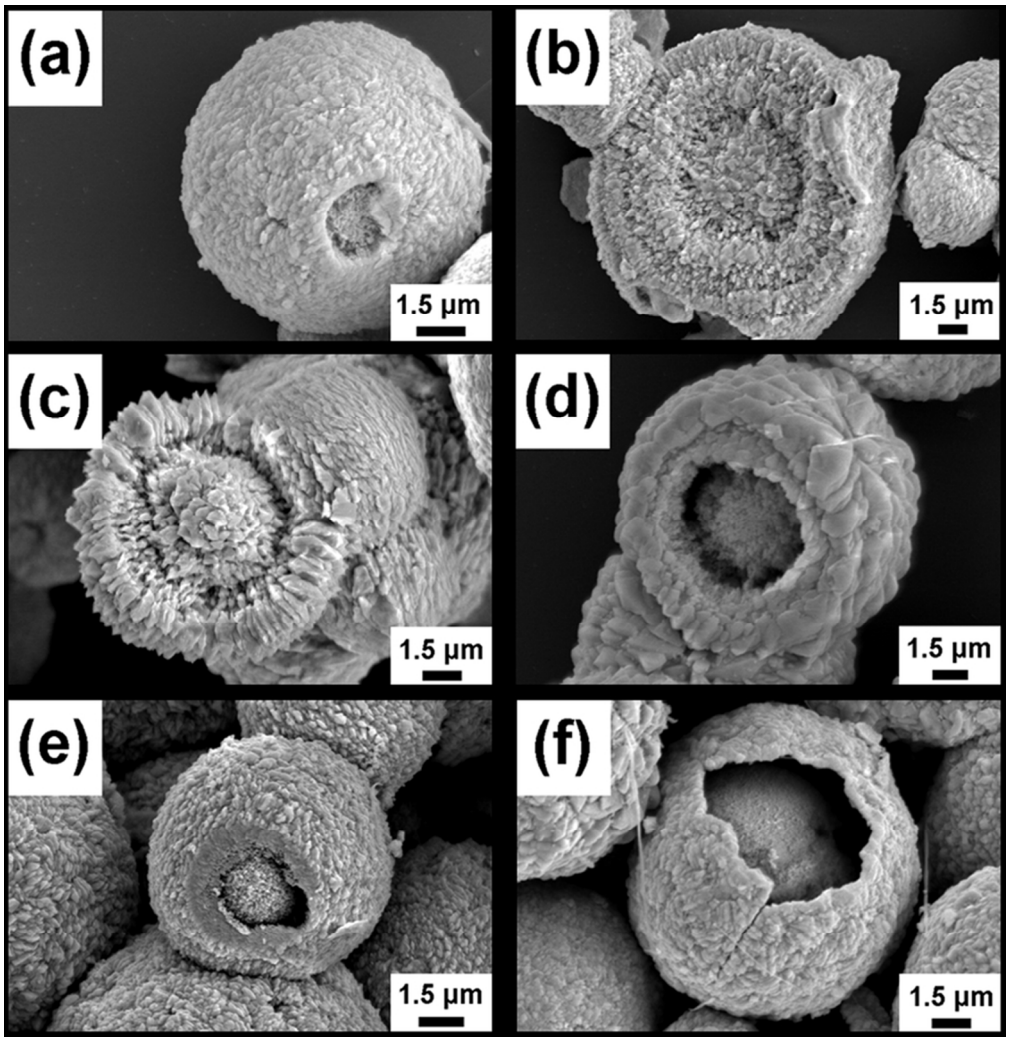

82x84mm (300 x 300 DPI)

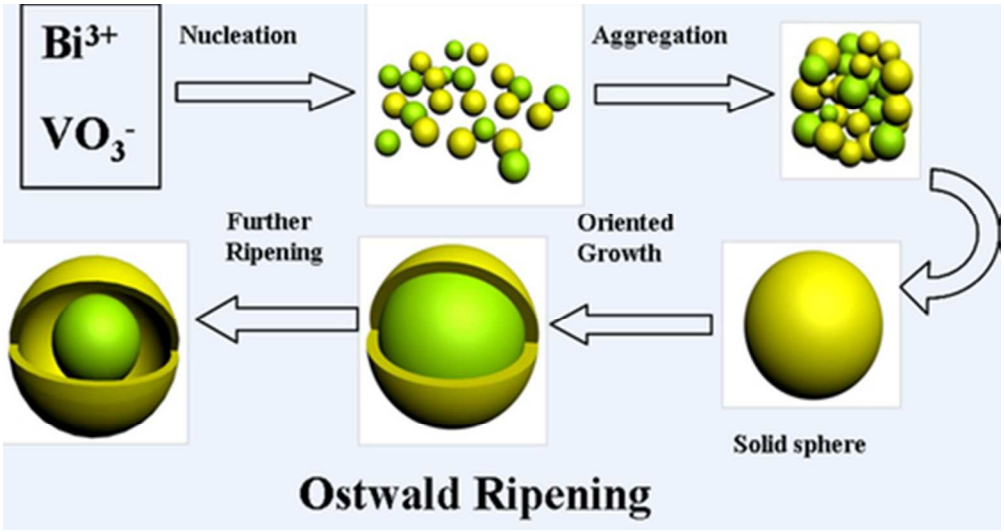

42x22mm (300 x 300 DPI)

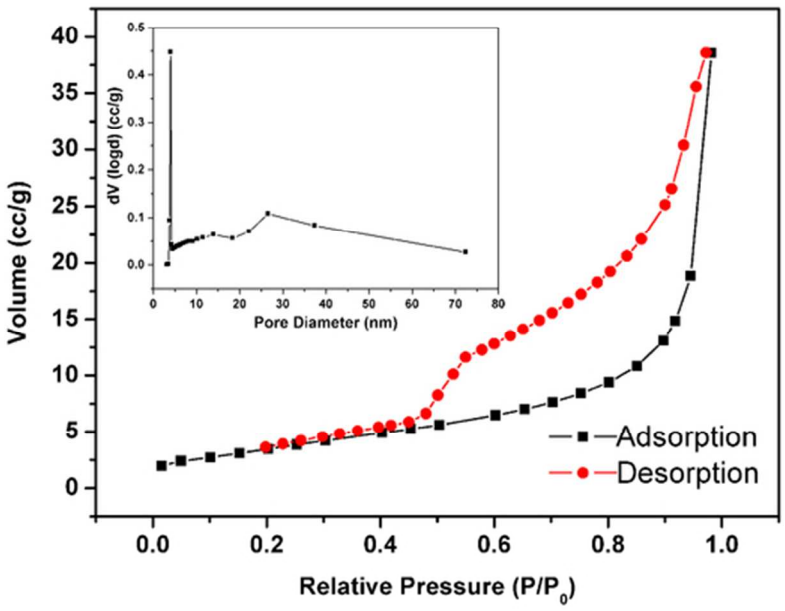

56x39mm (300 x 300 DPI)

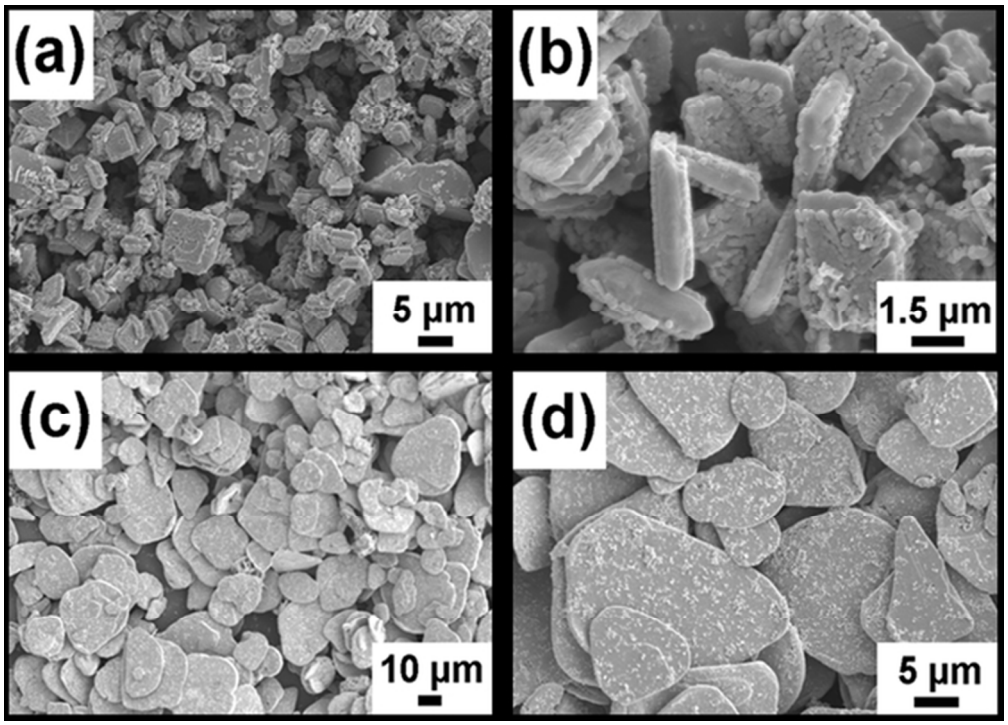

57x40mm (300 x 300 DPI)

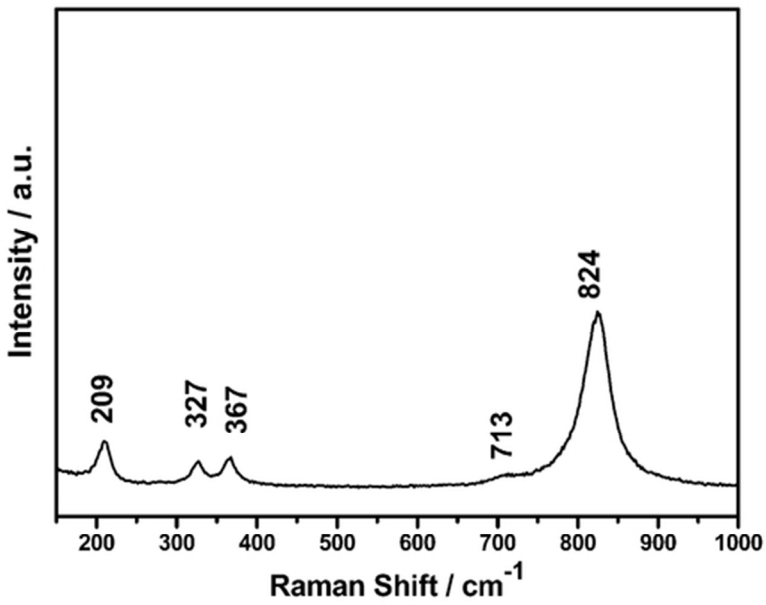

56x39mm (300 x 300 DPI)

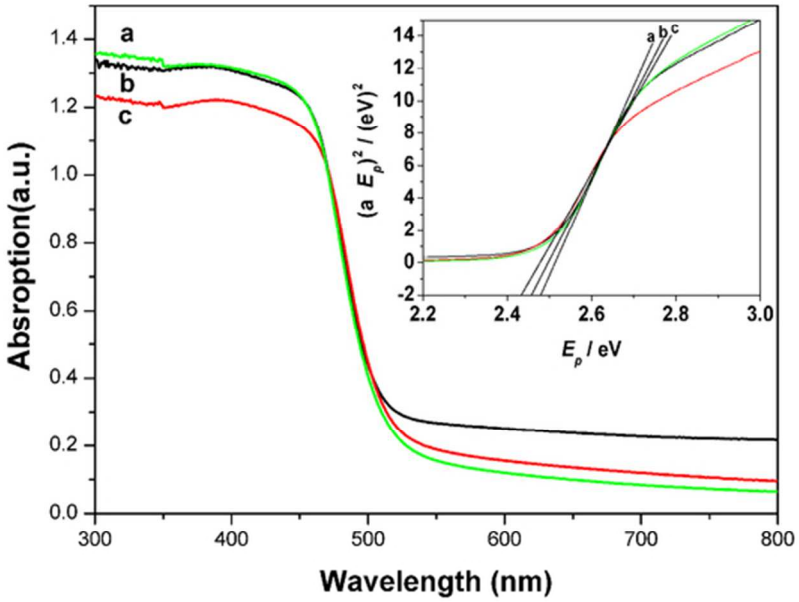

56x39mm (300 x 300 DPI)

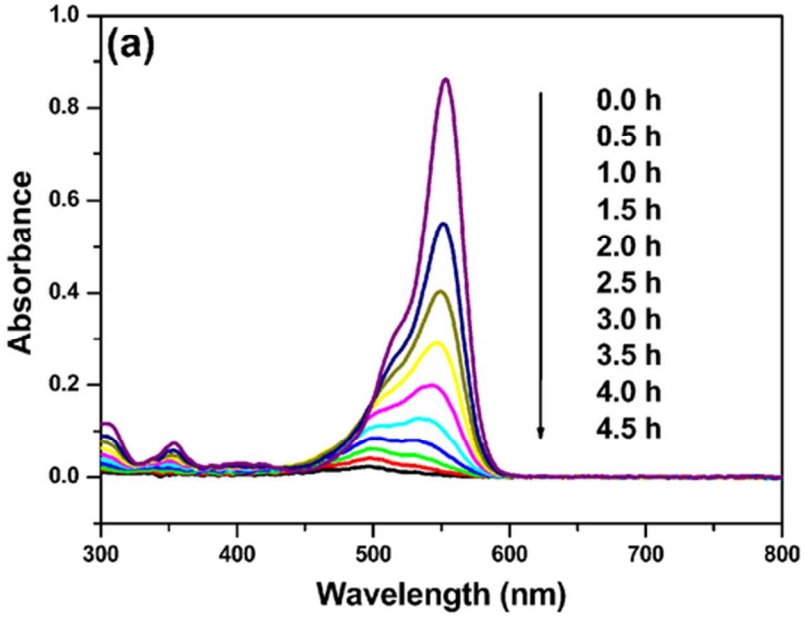

56x39mm (300 x 300 DPI)

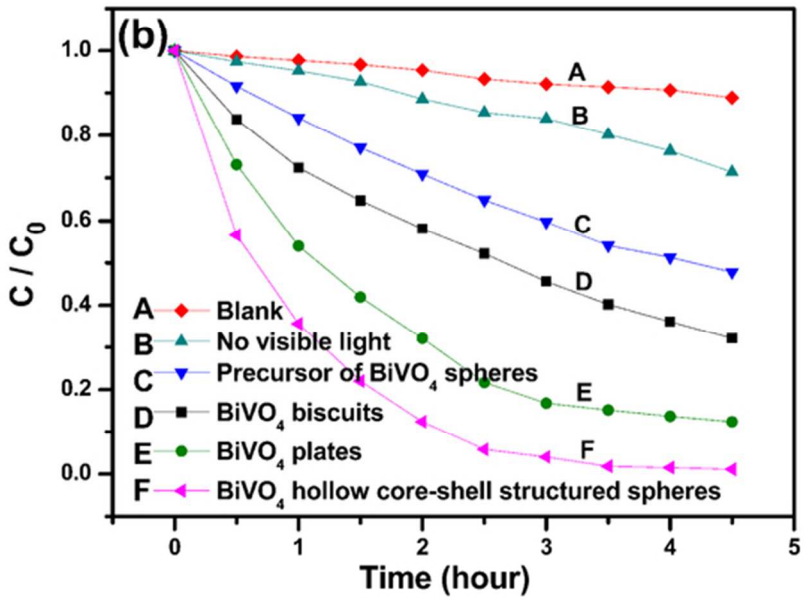

56x39mm (300 x 300 DPI)

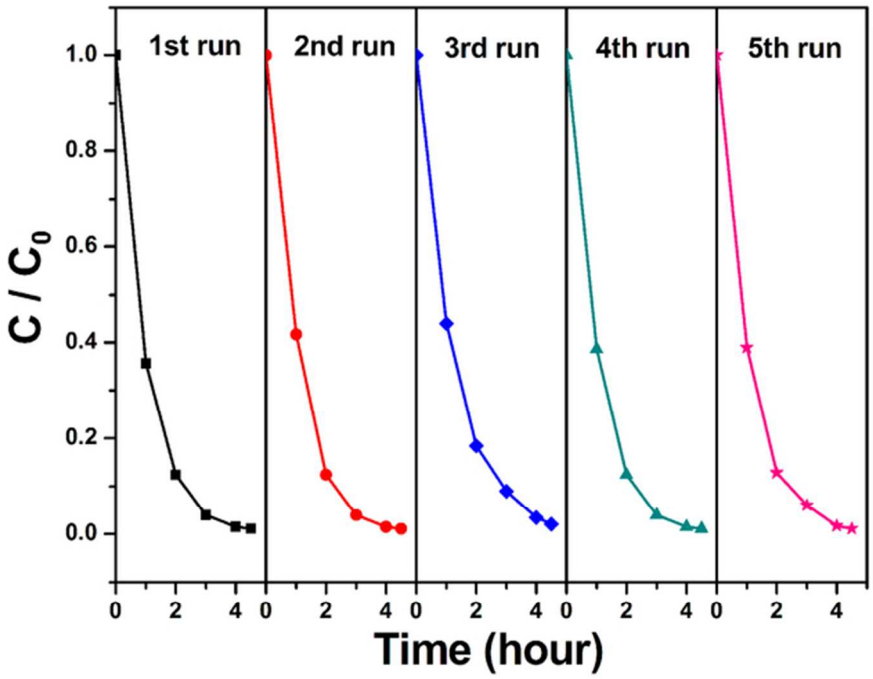

61x46mm (300 x 300 DPI)

A table of contents entry

Novel core-shell structured $BiVO_4$ hollow spheres with an ultra-high surface area as visible-light-driven catalyst

Yang Lu,[a] Yong-Song Luo,[a,b,*] Hong-Mei Xiao,[a] Shao-Yun Fu[a,*]

[†]Technical Institute of Physics and Chemistry, Chinese Academy of Sciences, Beijing 100190, China

[‡]Department of Physics and Electronic Engineering, Xinyang Normal University, Xinyang 464000, China

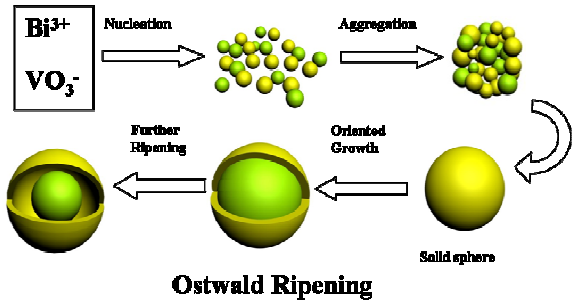

Novel core-shell-structured $BiVO_4$ hollow spheres synthesized via a simple hydrothermal route exhibit an excellent photocatalytic activity.